Biomaterials Science

ROYAL SOCIETY OF CHEMISTRY

PAPER

View Article Online
View Journal | View Issue

Cite this: *Biomater. Sci.*, 2025, **13**, 2012

An immunomodulatory encapsulation system to deliver human iPSC-derived dopaminergic neuron progenitors for Parkinson's disease treatment†

Emily A. Atkinson, *[a,b] Holly N. Gregory, [a,b] Lara N. Carter,[a,b] Rachael E. Evans,[a,b] Victoria H. Roberton, [a,b] Rachael Dickman [a] and James B. Phillips *[a,b]

Parkinson's disease is a neurodegenerative condition associated with the progressive loss of dopaminergic neurons. This leads to neurological impairments with heightening severity and is globally increasing in prevalence due to population ageing. Cell transplantation has demonstrated significant promise in altering the disease course in the clinic, and stem cell-derived grafts are being investigated. Current clinical protocols involve systemic immunosuppression to prevent graft rejection, which could potentially be avoided by encapsulating the therapeutic cells in a locally immunosuppressive biomaterial matrix before delivery. Here we report the progression of an immunomodulatory encapsulation system employing ultrapure alginate hydrogel beads alongside tacrolimus-loaded microparticles in the encapsulation of dopaminergic neuron progenitors derived from human induced pluripotent stem cells (hiPSCs). The hiPSC-derived progenitors were characterised and displayed robust viability after encapsulation within alginate beads, producing dopamine as they matured *in vitro*. The encapsulation system effectively reduced T cell activation (3-fold) and protected progenitors from cytotoxicity *in vitro*. The alginate bead diameter was optimised using microfluidics to yield spherical and monodisperse hydrogels with a median size of 215.6 ± 0.5 μm, suitable for delivery to the brain through a surgical cannula. This technology has the potential to advance cell transplantation by locally protecting grafts from the host immune system.

Received 25th November 2024,
Accepted 20th February 2025

DOI: 10.1039/d4bm01566e

rsc.li/biomaterials-science

Introduction

Parkinson's disease is a progressive neurodegenerative condition affecting at least 1% of the population over 65 years old and is characterised by the irreversible focal degradation of A9 dopaminergic neurons of the *substantia nigra pars compacta* in the ventral midbrain. The resulting dopamine deficiency leads to motor impairments including bradykinesia, rigidity, postural instability and rest tremors.[1] In addition, patients may present non-motor symptoms such as depression, anxiety, dementia, and insomnia.[2] Cases of Parkinson's disease are predicted to rise to 13 million worldwide by 2040,[3] emphasising the urgent need for effective therapies.

Cell therapy remains at the forefront of clinical and preclinical research into Parkinson's disease treatment. Dopaminergic neurons or their precursors are transplanted directly into the brain, with the intention that they eventually innervate the striatum and produce dopamine.[4] Clinical trials investigating this treatment have been undertaken since the 1980s, reporting a range of outcomes from graft-induced dyskinesias to patient benefits persisting for decades (reviewed by Barker *et al.*).[5] In earlier trials, the source of these cells was often human foetal ventral mesencephalic tissue, which while efficacious in some patients, presents practical and ethical issues for widespread adoption. Alternative cell sources with wider availability and potential for standardised production have been sought, with a particular focus on dopaminergic neural progenitors derived from human induced pluripotent stem cells (hiPSCs).[6]

Robust protocols have been developed to differentiate hiPSCs into dopaminergic progenitors *in vitro*, encompassing both embryonic and induced pluripotent stem cells.[7,8] Moreover, grafts derived from human pluripotent stem cells have produced functional improvements in rodent,[9,10] and primate models of Parkinson's disease.[11] A clinical trial of dopaminergic progenitors derived from hiPSCs for Parkinson's disease was initiated in 2018,[12] and derived from human embryonic stem cells in 2022 (STEM-PD).[13] In both cases, therapeutic cells were injected directly into the brain in suspension through a surgical cannula. Accordingly, this

[a]*UCL School of Pharmacy, University College London, London, UK.*
E-mail: emily.atkinson@ucl.ac.uk, jb.phillips@ucl.ac.uk
[b]*UCL Centre for Nerve Engineering, University College London, London, UK*
† Electronic supplementary information (ESI) available. See DOI: https://doi.org/10.1039/d4bm01566e

technology may advance Parkinson's disease treatment and alleviate the drawbacks of foetal tissue grafts.

Immunosuppression and graft protection are key aspects of cell grafting for Parkinson's disease, and this presents an opportunity for biomaterials to be explored as a way to improve the delivery of these therapeutics directly into the brain.[14] Although the brain has a degree of immune privilege, at least short-term immunosuppression is likely to be beneficial for graft survival.[15] Patients in major recent trials of foetal tissue have received systemic immunosuppression for approximately 12 months post-transplant.[16] Participants receiving the first iPSC-based therapy for Parkinson's disease (clinical trial ID: UMIN000033565) will be immunosuppressed with tacrolimus for 12 months.

Participants in the STEM-PD trial will also undergo a 12-month immunosuppressive regime, with the systemic delivery of tacrolimus, alongside other immunosuppressants.[13] Despite its necessity, the systemic administration of immunosuppressants (and tacrolimus in particular) in solid organ transplantation has been associated with substantial adverse effects including neuro- and nephrotoxicity, hypertension, and diabetogenesis.[17] Rather than systemically delivering immunosuppressants, local delivery of tacrolimus within a controlled-release formulation could be explored. This may reduce the associated side effects by vastly reducing the dosage required to protect the transplanted cells from the host immune system and minimise side effects.

Moreover, this local immune isolation approach could be extended by encapsulating the therapeutic cells within a semi-permeable hydrogel. This could act as a physical barrier against host immune cells whilst allowing the diffusion of oxygen and nutrients into the hydrogel for the survival of the encapsulated cells and the diffusion of dopamine and therapeutic factors out. Alginate has been extensively investigated in this capacity for the transplantation of pancreatic islet cells and has yielded immune protection of functional islets in both primates and humans.[18,19] Alginate hydrogels have been well characterised and can be formulated with the appropriate mechanical and physical properties for brain delivery.[20–23] A recent clinical trial investigated the intra-striatal delivery of alginate-encapsulated porcine choroid plexus cells in patients with Parkinson's disease. Although the efficacy of the transplanted cells was not established, the technology was determined to be safe and well-tolerated in humans.[24]

We have previously reported an immunoprotective cell encapsulation system comprised of an alginate hydrogel and tacrolimus-loaded nanoparticles, which displayed appropriate mechanical properties and permeability while maintaining the viability of encapsulated SH-SY5Y neuroblastoma cells over two weeks *in vitro*.[20] The present study progresses that technology by investigating the encapsulation of dopaminergic progenitors derived from hiPSCs, equivalent to those used in current clinical trials for Parkinson's disease. Furthermore, it aimed to optimise the volume and diameter of the alginate hydrogel beads for clinical translation by identifying a method of alginate bead production that maintains encapsulated cell viability, is suitable for passing through a surgical cannula for direct delivery into the brain (currently used in clinical trials) and has a diameter which avoids the formation of a necrotic core (<200 μm).[14]

In this work, dopaminergic neuron progenitors were incorporated into the alginate encapsulation system and combined with novel tacrolimus-loaded polycaprolactone microparticles manufactured using a more robust single emulsion technique. We hypothesised that encapsulating hiPSC-derived dopaminergic neuron progenitors in alginate beads with tacrolimus microparticles would modulate T cell responses and improve encapsulated cell survival in an *in vitro* model of T-cell mediated immune rejection. To test this hypothesis, we investigated the capacity of the biomaterial system to protect the dopaminergic neuron progenitors from a T cell response *in vitro*, alongside its ability to modulate T cell population number. The technology was compared with unencapsulated cells and cells encapsulated in alginate only. Finally, the production methodology for alginate beads was optimised using a coaxial flow reactor to reduce their size and improve homogeneity.

Materials and methodology

Materials

The ESI (ESI Tables 1 and 2†) contains details on materials including suppliers and catalogue numbers.

hiPSC differentiation and characterisation

Differentiation of hiPSCs into dopaminergic neuron progenitors. Human induced pluripotent stem cells (hiPSCs, CGT-RCiB-10) derived from CD34+ peripheral blood cells were supplied by the Cell and Gene Therapy Catapult, UK. hiPSCs were provided at passage 35 and used up to passage 50. Cells were expanded and maintained on vitronectin-coated flasks (0.5 μg cm^{-2}) in Essential 8/Essential 8 flex media and passaged 1 : 4 at 80% confluency. All cultures were maintained in a humidified incubator at 37 °C with 5% CO_2. hiPSCs were differentiated into dopaminergic neuron progenitors (day 16), then mature dopaminergic neurons (day 35) adapting the protocol from Kirkeby *et al.* in Scheme 1 and Table 1.[7,8]

In summary, on day 0, hiPSCs were passaged with EDTA (0.5 mM) then cultured in Neural Induction Medium (NIM) (Table 1) and supplemented with Y-27632 (10 μM), SB431542 (10 μM), Noggin (100 ng mL^{-1}), CHIR99021 (200 ng mL^{-1}) and SHH-C24II (200 ng mL^{-1}). On day 2, cells were suspended in the same media without Y-27632, and began to form embryoid bodies. During this time, plates were coated with poly-L-ornithine (PLO) in H_2O (15 μg mL^{-1}) and were incubated for 48 h at 37 °C. Wells were then washed with H_2O thrice then fibronectin (0.5 mg mL^{-1}) and laminin (5 μg mL^{-1}) in PBS were added for a further 48 h at 37 °C. On day 4, cells were seeded onto the coated plates and cultured in Neural Proliferation Media (NPM) (Table 1) plus SB431542 (10 μM), Noggin (100 ng mL^{-1}), CHIR99021 (200 ng mL^{-1}) and

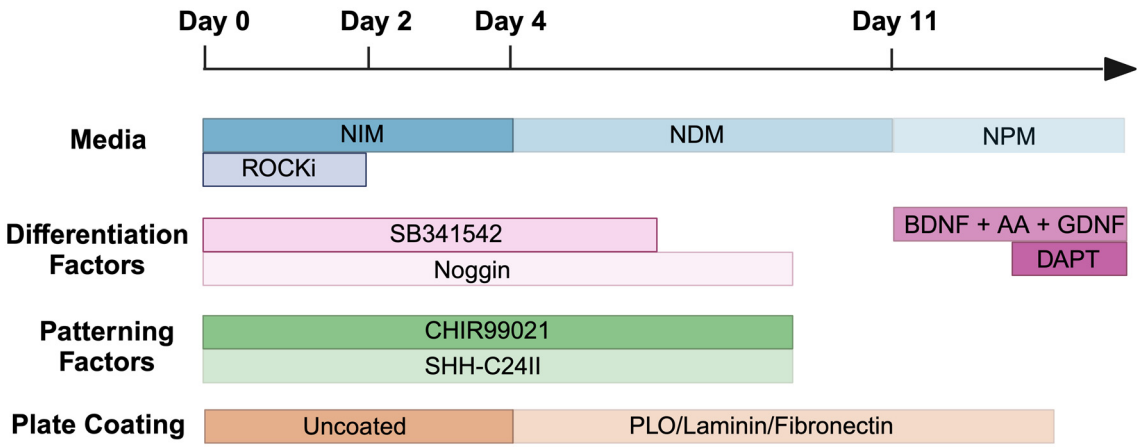

Scheme 1 Schematic of differentiation methodology from hiPSCs to dopaminergic neurons, adapted from Kirkeby *et al.*[7,8] Abbreviations include neural induction media (NIM), neural differentiation media (NDM), neural proliferation media (NPM), ROCK inhibitor (ROCKi), brain-derived neurotrophic factor (BDNF), ascorbic acid (AA), glial cell line-derived neurotrophic factor (GDNF), poly-L-ornithine (PLO).

Table 1 Media composition for differentiation of hiPSCs into dopaminergic neurons

Neural induction media (NIM)	Neural proliferation media (NPM)	Neural differentiation media (NDM)
DMEM/F12: Neurobasal (1 : 1)	DMEM/F12: Neurobasal (1 : 1)	Neurobasal
1× N2 (1 : 100)	0.5× N2 (1 : 200)	
1× B27 (1 : 50)	0.5× B27 (1 : 100)	1× B27 (1 : 50)
2 mM L-glutamine (1 : 100)	2 mM L-glutamine (1 : 100)	2 mM L-glutamine (1 : 100)

SHH-C24II (200 ng mL^{-1}). On day 11, cells were replated onto coated plates and media changed to Neural Differentiation Medium (NDM) (Table 1) plus GDNF (10 ng mL^{-1}), BDNF (20 ng mL^{-1}) and ascorbic acid (0.2 mM). On day 14 the medium was replaced, with the addition of DAPT (1 μM), and cells were maintained in this medium for future use (Scheme 1).

Dopamine ELISA. Conditioned media was collected from undifferentiated hiPSCs, dopaminergic neuron progenitors at day 16, and mature dopaminergic neurons at day 35 of differentiation. Cells were seeded at 1×10^6 cells per well in a 6-well plate for 24 hours, whereafter the media was collected and stored at −20 °C. A dopamine ELISA (Elabscience®) was used, directly following the manufacturer's instructions, and all incubations were carried out at 37 °C. Briefly, the standard or sample (50 μL) and the biotinylated detection antibody (50 μL) were added to each well and incubated for 45 minutes, then wells were washed thrice with wash buffer (350 μL), and HRP conjugate (100 μL) was added. The plate was incubated for 30 minutes, then the substrate reagent (90 μL) was introduced followed by a further incubation for 15 minutes, and finally the reaction was terminated by addition of stop solution (50 μL). Optical density (OD) of the samples was read immediately at 450 nm on a Synergy™ HTX Multi-Mode Microplate Reader.

Cytokine array. Conditioned media collected for the dopamine ELISA was also used in the cytokine array. A human cytokine array kit (R&D Systems) was used according to the manufacturer's instructions. Briefly, array buffer (2 mL) was added to each membrane and incubated for 1 h with shaking at room temperature (RT), then removed. Array buffer (0.5 mL) and a human cytokine array detection antibody cocktail (15 μL) were added to each media sample (1 mL), and incubated for 1 h at RT. This mixture was then added to each membrane and incubated overnight at 4 °C with shaking. Membranes were washed thrice and incubated in streptavidin-HRP (2 mL) for 30 minutes at RT with shaking, then washed again. Finally, Chemi Reagent mix (1 mL) was added to each membrane and incubated for 1 minute before imaging using a SynGene GeneGnome Imaging system. Quantification was carried out using ImageJ software, where mean pixel density was determined for each cytokine or chemokine from duplicate antibody spots.

Immunofluorescence. Cells in monolayer on coverslips were fixed with 4% paraformaldehyde at 4 °C overnight and permeabilised with Triton-X-100 (0.1%) in PBS. Cells were washed thrice in PBS then blocked using 5% normal goat or horse serum in PBS for 15 minutes at RT, where the choice of blocking serum was matched to the species in which the secondary antibody was raised. Cells were washed in PBS then incubated with the primary antibody for either 90 minutes at RT or overnight at 4 °C (Table 2). Cells were then washed as previously described and incubated with the secondary antibody for 45 minutes at RT (Table 2). Cells were washed again, then mounted using VECTASHIELD® Hardset™ Antifade Mounting Medium with DAPI (Vector laboratories #H-1500) on glass slides. Cells were imaged using a fluorescence microscope under ×10 and ×20 objectives (Zeiss AxioLab.A1 with AxioCam CM1), and quantification of those immunoreactive for a specific marker was conducted using ImageJ software.

Table 2 Antibodies used in immunocytochemical characterisation of hiPSC differentiation

Antibody	Dilution
β-III-Tubulin (raised in rabbit)	1 : 300
β-III-Tubulin (raised in mouse)	1 : 300
LMX1A (raised in rabbit)	1 : 400
Nestin (raised in mouse)	1 : 400
OCT3/4 (raised in goat)	1 : 100
Tyrosine Hydroxylase (raised in mouse)	1 : 500
Dylight 488 horse anti-mouse IgG	1 : 400
Dylight 594 goat anti-rabbit IgG	1 : 400
Dylight 594 horse anti-mouse IgG	1 : 400
Dylight 594 horse anti-goat IgG	1 : 200
Goat anti-mouse Alexa Fluor Plus 488	1 : 200
Goat anti-rabbit Alexa Fluor Plus 594	1 : 200

Tacrolimus-loaded microparticles

Fabrication by single-emulsion. Polymeric microparticles loaded with the immunosuppressant tacrolimus were generated using a single emulsion technique. A 2% polyvinyl alcohol (PVA) solution was prepared by adding 13–23 kDa PVA (5 g) to distilled water (250 mL) with stirring overnight, followed by filtration through a 0.2 μm syringe filter. A polymer and drug solution was prepared by combining 20% 45 kDa polycaprolactone (PCL) in dichloromethane (5 mL) with 100 mg mL^{-1} tacrolimus in ethyl acetate (500 μL). To form the microparticles, 200 mL of the 2% PVA solution was first introduced to a 250 mL beaker and homogenisation started at 10 000 rpm using a Silverson high-speed laboratory mixer. The solution containing polymer and drug was streamed into the emulsifier over 7–9 seconds, and then mixing continued for two minutes. The mixture was then stirred at 500 rpm for four hours, before being filtered through a 100 μm cell strainer. The microparticles were then washed with excess distilled water and collected *via* centrifugation (3 minutes, 3000 rpm). After repeating this step five times, the particles were frozen in liquid nitrogen and freeze-dried for 72 hours, prior to storage at −20 °C.

Characterisation of morphology and release kinetics. To investigate morphology with scanning electron microscopy, freeze-dried microparticles were first added to a carbon tab and sputter-coated with gold for one minute using a Q150R coater (Quorum). Microparticles were imaged at ×2000 using an accelerating voltage of 10 kV on a Phenom™ Pro G6 Desktop SEM (Thermo Fisher Scientific), and diameter was determined using approximately 90 measurements per image across three pre-determined fields.

To assess the drug release profile, 20.0 mg of microparticles (n = 3) were added to 50 mM ammonium bicarbonate release buffer (1 mL) in microtubes and placed in a shaking incubator at 37 °C and 75 rpm. Every 2–3 days the microtubes were centrifuged at 12 500 rpm for five minutes, the buffer completely removed and then replaced with fresh buffer. Release samples were stored at −20 °C until analysis.

The concentration of tacrolimus in the release buffer was determined using ultra-high performance liquid chromatography tandem mass spectrometry (UHPLC-MS/MS), with a Shimadzu Nexera X2 UHPLC/Shimadzu LCMS 8060 and a Phenomenex Kinetex C8 (50 × 2.1 mm) column with 5 μm pore size, with the column oven set at 50 °C. The mobile phase used for analysis comprised water with 0.1% formic acid (A) and acetonitrile : water (95 : 5) with 0.1% formic acid (B) under gradient elution according to Table 3, with a flow rate of 0.4 mL min^{-1}. An internal standard of tolbutamide in acetonitrile (500 ng mL^{-1}) was used in all calibration samples, standards and blanks.

Cell encapsulation system and *in vitro* efficacy

Production of alginate beads. Dopaminergic neuron progenitors (day 16) were detached from the plates with accutase and resuspended in ultra-pure 2% sodium alginate solution (20 mg PRONOVA SLM100 sodium alginate in 1 mL Dulbecco's Minimum Essential Medium) at 1 × 10^6 cells mL^{-1}. The cell solution was loaded into a syringe attached to a 31G needle, mounted onto a syringe pump, and then dispensed into a bath of 102 mM $CaCl_2$ in ddH_2O at 25 mL h^{-1} from a height of 3 cm, with stirring at 150 rpm. The formed alginate beads were left to crosslink in $CaCl_2$ for 20 minutes, whereafter the bath solution was aspirated and the beads were washed with 1% saline then maintained in culture media.

Live/Dead™ assay

At 24 h after encapsulation, cells were stained using a Live/Dead™ Cell Imaging Kit (Thermo Fisher #04511) as per the manufacturer's instructions to assess cell viability. In darkness, encapsulated cells were washed with PBS and incubated with the staining solution (1 : 1000) for 15 minutes at 37 °C. The staining solution was removed and cells were washed with culture media. Cells were counted from three planes in at least three alginate beads per experimental group using a fluorescence microscope (Zeiss Axiolab.A1).

T cell isolation, purification and culture

Human CD3+ T cells were isolated from human peripheral blood mononuclear cells (PBMCs). T cells were separated using the EasySep™ Human CD3 Positive Selection Kit II (STEMCELL™ Technologies) by following the manufacturer's instructions. In brief, the selection cocktail (100 μL) was added to PBMCs (1 × 10^8 cells per mL) and incubated at RT for three minutes. RapidSpheres™ (60 μL mL^{-1}) were introduced to the

Table 3 LCMS mobile phase gradient for determination of tacrolimus concentration in release samples

Time (min)	Solvent A: Water with 0.1% formic acid (%)	Solvent B: Acetonitrile: Water (95:5) with 0.1% formic acid: (%)
0	98	2
0.3	98	2
1.1	5	95
1.75	5	95
1.8	98	2
2.5	98	2

PBMCs and incubated for a further three minutes at RT. RPMI-160 medium with 1% penicillin/streptomycin/S, 1% L-glutamine, 1% non-essential amino acids and 10% fetal bovine serum (to 2.5 mL) was added and the T cells were extracted using a magnet for three minutes. The supernatant was removed, and the extraction process was repeated thrice. Cells were cultured for up to two weeks in the RPMI-based media.

T cell assay

T cells were seeded into 12-well plates (40 000 cells per well) containing no cells, unencapsulated dopaminergic neuron progenitors (50 000 cells per well), encapsulated dopaminergic neuron progenitors, or encapsulated dopaminergic neuron progenitors with tacrolimus-loaded PCL microparticles (0.25 mg). Cultures were monitored over five days using the Sartorius Incucyte® Live-Cell Analysis instrument and the number of T cells in each condition was determined at the end of the experiment using a haemocytometer. The viability of the dopaminergic neuron progenitors was measured using the LIVE/DEAD™ assay, as described above.

Alginate bead size optimisation

Conical tip needles. Optimisation of alginate bead size was performed using 2% sodium alginate solution without cells. Alginate beads were produced as above, and the dispensing syringe was fitted with needles of various internal diameters (18G, 22S, 24G, 26S and 31G all point style 5 with conical tip). The alginate concentration had been previously optimised to match the biomechanical properties of the brain so remained unchanged.[20]

Pulled glass pipettes. To further reduce alginate bead size, pulled glass pipettes with smaller internal diameters (100 μm, 80 μm, 60 μm, 40 μm and 20 μm) were also used to dispense the alginate solution. Pipettes were pulled using a Flaming/Brown micropipette puller at 630 °C and a velocity of 20 m s^{-1} then broken by hand to the required diameters. In this setup, the syringe was connected to a 21G butterfly IV cannula, attached to the glass pipette with parafilm, and clamped above the $CaCl_2$ bath. Pipette tips were coated with Tween 20 to reduce surface tension with the alginate solution, but all other parameters remained the same.

Analysis. Photographs were taken of the alginate beads alongside a ruler and the diameter was measured with ImageJ.[25]

Microfluidics. Alginate beads were also generated by microfluidics, using a coaxial flow reactor created in-house. To assemble the reactor, a glass capillary (internal diameter 0.595 mm, length 54 mm) was first placed into a glass tube (internal diameter 1.6 mm, length 162 mm). A PEEK T-junction was fitted to the system with two inlets and gaskets attached to plastic HPLC tubing (internal diameter 74 mm), each controlled with a syringe pump (World Precision Instruments). This allowed the 2% alginate solution to flow through the inner microcapillary (core solution) while sunflower oil flowed through the outer tube, and the two continuous, immiscible fluid streams came into contact at the end of the microcapillary and flowed through the reactor. The alginate and sunflower oil mixture was collected into a 1.5 mL Eppendorf tube containing $CaCl_2$ (500 μL, 102 mM) and cross-linked for 30 minutes. The flow rate ratio (1 : 3–1 : 20) and flow rates of both alginate (10–40 μL min^{-1}) and sunflower oil (100–400 μL min^{-1}) were optimised. The alginate beads were then washed with hexane (3 × 1 mL) and PBS (3 × 1 mL). The alginate bead size was measured by laser diffraction (Mastersizer). Images were taken at ×10 using a phase contrast light microscope (EVOS), and alginate beads were measured with ImageJ.[25]

Data analysis

Normality was determined using the Shapiro–Wilk test. If normal distribution was shown then either a 1- or 2-way statistical analysis of variance (ANOVA) was used as appropriate with a *post-hoc* test by either a Dunnett's, Tukey's or Bonferroni multiple comparison test. Degrees of significance were assessed by four different rating values: $*p < 0.05$, $**p < 0.01$ $***p < 0.001$ and $****p < 0.0001$.

Results

CGT-RCiB-10 hiPSCs were differentiated first into dopaminergic progenitors (day 14–16) then dopaminergic neurons (day 35) using an established protocol.[7] Cell phenotype was assessed using phase contrast imaging and immunocytochemistry, alongside dopamine production and cytokine release. Cell morphology changed markedly over 16 days in the presence of various patterning factors (Fig. 1). Day 0 hiPSCs formed small colonies with hexagonal cell morphology (yellow arrow), and by day 2–4, floating embryoid bodies were formed (red arrow). On day 4, these cell clusters were triturated and attached to a laminin and PLO-coated plate. By day 14–16, through exposure to various factors, the cells displayed a spiny morphology with neural network formation (purple arrows) which are typical of dopaminergic progenitors.

Differentiation was also assessed using immunocytochemistry, comparing undifferentiated hiPSCs with hiPSC-derived dopaminergic progenitors (day 16) and mature dopaminergic neurons (day 30–35). hiPSCs expressed the pluripotency marker Oct4 alongside the neural stem cell marker Nestin, and day 16 dopaminergic progenitors were positive for the neuronal cytoskeletal protein βIII-tubulin. At day 30–35 of differentiation, cells also expressed βIII-tubulin and LMX1A (Fig. 2A). Further immunocytochemistry on day 16 revealed that dopaminergic progenitors also expressed the midbrain dopaminergic neuron marker LMX1A with nuclear localisation at this time point, as well as tyrosine hydroxylase (TH) (Fig. 2B).

Thereafter, the concentration of dopamine in the secretome of these cultures was determined by ELISA to confirm the dopaminergic functionality of the neurons generated by this protocol (Fig. 3A). The day 35 hiPSC-derived dopaminergic

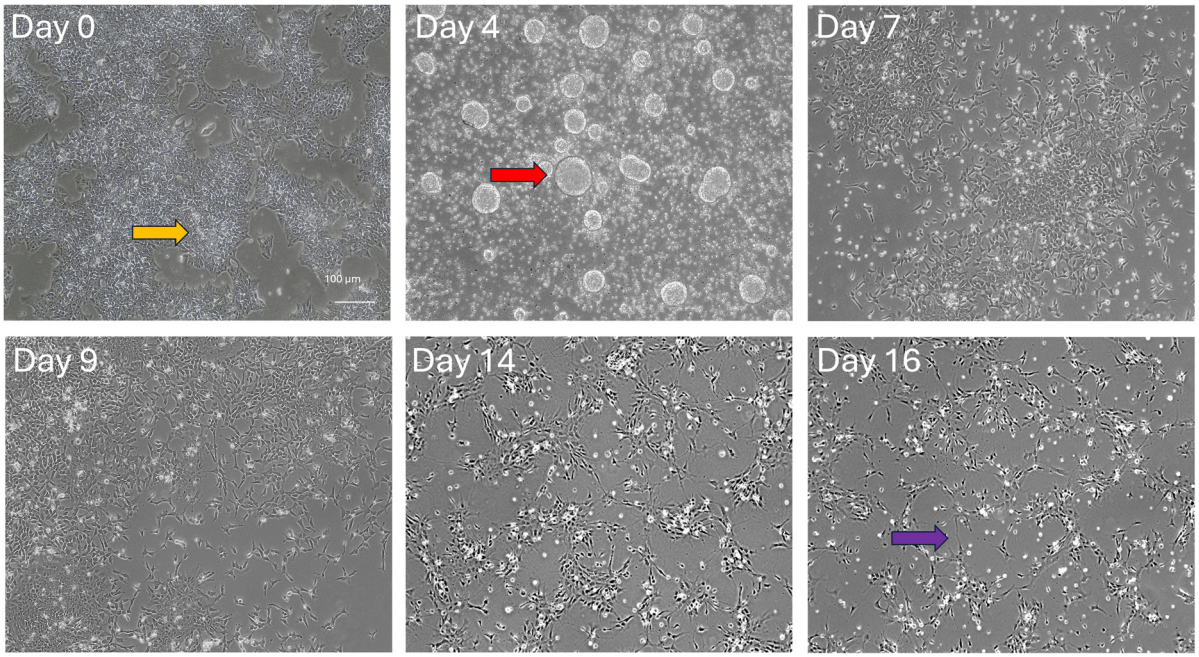

Fig. 1 Differentiation of hiPSCs into dopaminergic progenitors. Phase contrast micrographs displaying hiPSCs (yellow arrow) formed embryoid bodies (red arrow) between days 1 and 4, and dopaminergic progenitors formed a network of interconnecting neurites (purple arrows) by day 14. Scale bars = 100 µm.

neuron secretome contained 217 ± 31.7 pg mL^{-1} dopamine, amounting to a seven-fold increase ($p < 0.0001$) over the 29.1 ± 6.1 pg mL^{-1} dopamine detected from undifferentiated hiPSCs. The secretome from each cell population was also analysed for the presence of 36 individual human cytokines and chemokines, of which four were detected (Fig. 3B and Fig. S1†). CCL5, CXCL12, IL-1β and CD40 were all present in hiPSC secretome, where levels of CCL5 were highest. The concentration of this chemokine was reduced in both the day 16 dopaminergic progenitor and day 35 dopaminergic neuron secretome, and IL-1β was undetectable in these cultures. In comparison, levels of CXCL12 were elevated in the differentiated cell types and CD40, while present in day 16 progenitor culture media, was absent in day 35 dopaminergic neuron media.

To protect the grafted progenitors from the host immune system pharmacologically, polycaprolactone microparticles loaded with the immunosuppressant tacrolimus were manufactured, for use in conjunction with the encapsulation system (Fig. 4). A single emulsion fabrication technique was employed, which generated discrete and spherical microparticles (Fig. 4A), with an average diameter of 6.98 ± 0.33 µm (mean ± SEM) and a maximum diameter of 29.41 µm (Fig. 4B). Tacrolimus was eluted from the microparticles in a sustained manner, reaching a cumulative total of 900 ng of immunosuppressant released per milligram of material over three weeks (Fig. 4C).

The effect of encapsulation within alginate beads on the viability of dopaminergic progenitors was explored, alongside the capacity of the immunomodulatory encapsulation system to protect these cells in an *in vitro* model of immune response (Fig. 5). Day 16 hiPSC-derived dopaminergic progenitors were encapsulated within alginate beads, generated by dropwise release from a 31 G needle and crosslinking in a $CaCl_2$ bath (Fig. 5A). The viability of the progenitors 24 hours after encapsulation was 79.58 ± 1.4%, a small but significant reduction compared to unencapsulated cells at 91.31 ± 0.92% ($p < 0.0001$) (Fig. 5B).

Cultures of mismatched human T cells were then introduced to either unencapsulated day 16 dopaminergic progenitors, progenitors encapsulated in alginate beads, or progenitors encapsulated in alginate beads alongside tacrolimus microparticles (Fig. 5C). After five days, unencapsulated progenitors had 0% viability. Progenitors encapsulated in alginate displayed 49.08 ± 1.97% viability (±SEM), which significantly increased to 65.7 ± 3.61% with the addition of tacrolimus microparticles ($p < 0.0005$) (Fig. 5D). The number of T cells cocultured with the unencapsulated dopaminergic neuron progenitors increased 6.6-fold from 40 000 cells per well at the start of the experiment to 265 750 ± 31 100 (±SEM). The number of T cells increased to a lesser 4.5-fold extent, 180 717 ± 21 912 (±SEM), when cells were encapsulated in alginate and the increase was only 2-fold, 83 583 ± 12 569 (±SEM), with the addition of tacrolimus-loaded microparticles (Fig. 5E). Phase contrast images showed the co-culture of unencapsulated T cells and unencapsulated dopaminergic neuron progenitors on day 0 of the assay (Fig. 5F), and day 5 of the assay (Fig. 5G) at which point no dopaminergic neurons were observed to survive.

To enhance the clinical relevance of this technology, the encapsulation process was optimised to produce smaller and

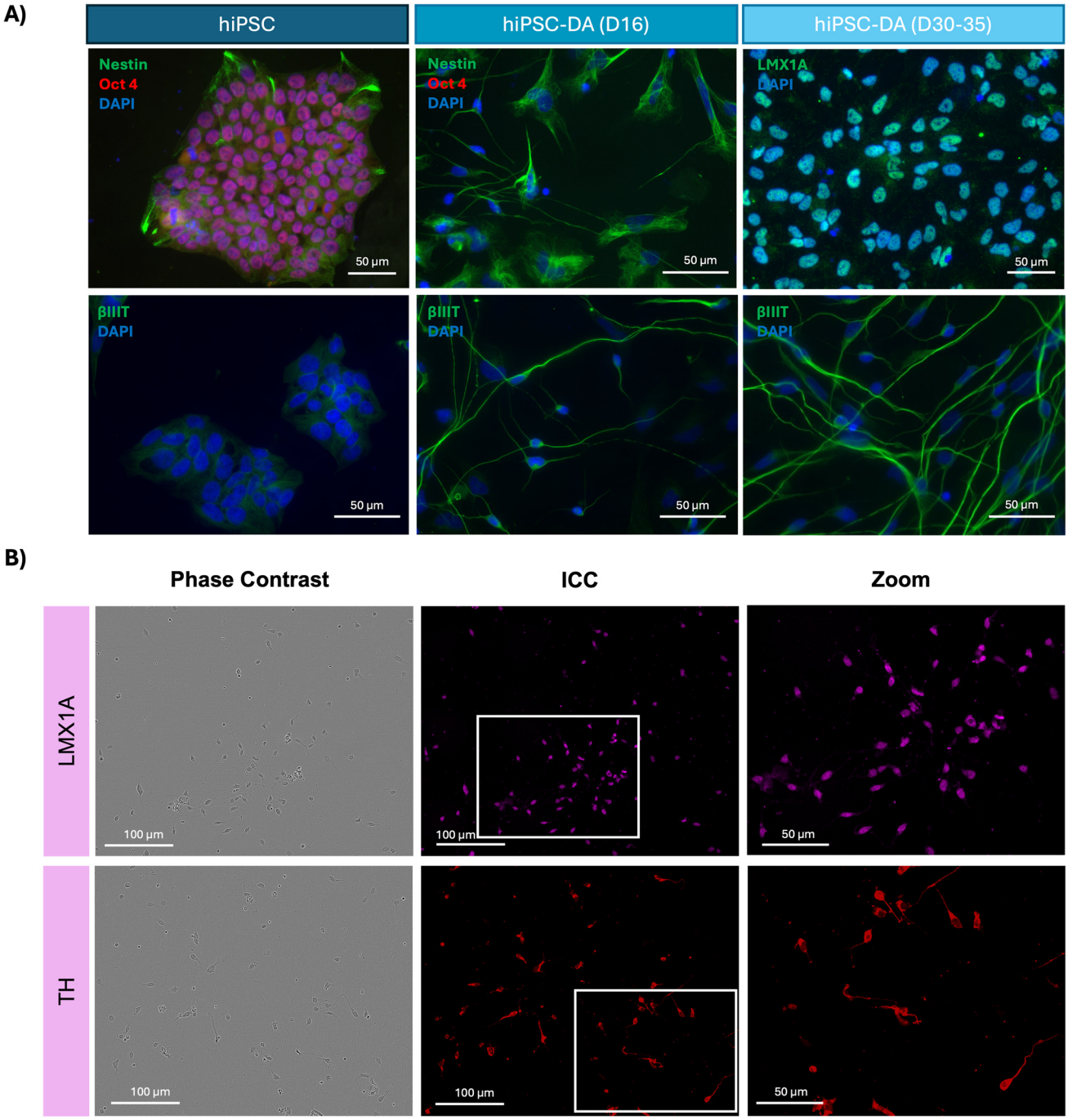

Fig. 2 Immunocytochemistry analysis of hiPSCs, dopaminergic progenitors and dopaminergic neurons. (A) Fluorescence micrographs demonstrating hiPSCs express the pluripotency marker Oct4 and neural stem cell marker Nestin, day 16 hiPSC-DAs express neuronal marker βIII-tubulin, and day 35 hiPSC-DAs express βIII-tubulin and midbrain dopaminergic neuron marker LMX1A. (B) Phase contrast images and fluorescence micrographs displaying day 16 hiPSC-DAs express and midbrain dopaminergic neuron marker LMX1A and the dopaminergic neuron marker tyrosine hydroxylase (TH).

more consistent alginate beads (Fig. 6). Initially, the same syringe pump system and associated conditions were employed, and the alginate solution was extruded through needles of decreasing diameter (Fig. 6A). A reduction in median alginate bead size was observed with reducing needle diameter (Fig. 6B). The median alginate bead diameter decreased almost three-fold from 2475 μm using an 838 μm (internal diameter) needle, to 895 μm using a 133 μm needle. However, all needles produced a wide range of bead diameters – the smallest range was 45 μm, obtained with the 133 μm needle,

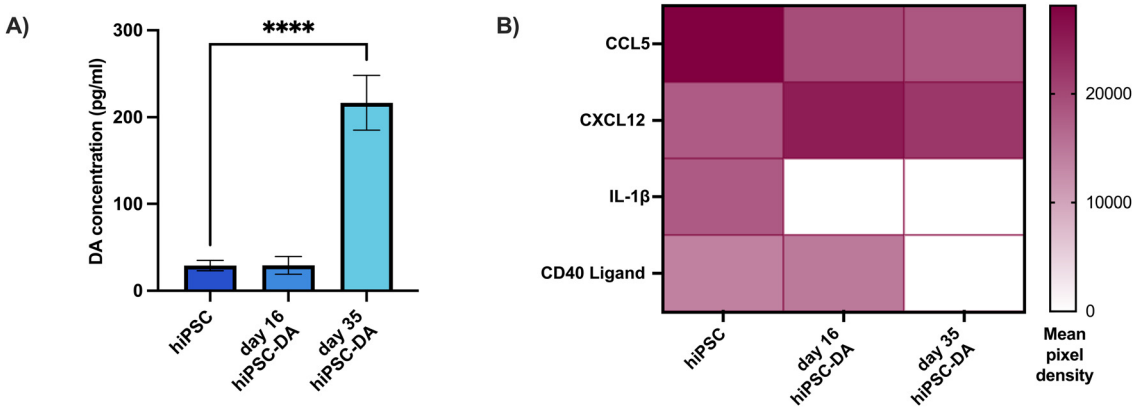

Fig. 3 Dopamine production and cytokine array for hiPSCs, dopaminergic progenitors and functional dopaminergic neurons. (A) *In vitro* dopamine production was significantly increased in day 35 hiPSC-DAs compared with undifferentiated hiPSCs (one-way ANOVA with Dunnett's *post-hoc* test, $n = 3$, mean ± SD, **** $p < 0.0001$). (B) Heat map illustrating the detection of cytokines in the secretome throughout differentiation towards dopaminergic neurons. Data expressed as the mean of the two spots on the array for each cytokine ($n = 1$).

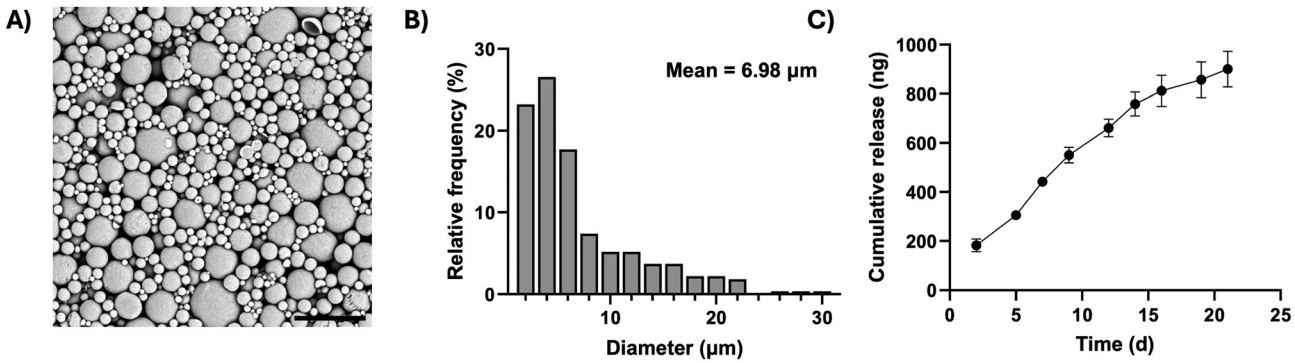

Fig. 4 Synthesis and characterisation of tacrolimus-loaded microparticles. (A) Scanning electron micrograph of tacrolimus-loaded microparticles, scale bar = 30 µm. (B) Frequency distribution of microparticle diameter from scanning electron micrographs ($n = 3$ images, ~90 measurements per image). (C) Cumulative release of tacrolimus per mg of microparticles over three weeks ($n = 3$ samples ± SD).

and the largest was 1950 µm, using the 413 µm needle. To explore how far the correlation between needle diameter and bead size continued, pulled pipettes with smaller, decreasing internal diameters were investigated (Fig. 6C), showing a gradual decrease in alginate bead diameter from 1957 ± 197 µm with a 100 µm pipette to 1111 ± 322 µm with a 10 µm pipette (Fig. 6D).

To further decrease the alginate bead size and improve homogeneity, a coaxial flow reactor was created to generate hydrogel beads using microfluidics (Fig. 7). The reactor utilised a continuous phase of sunflower oil and a disperse phase of 2% alginate at various flow rates and flow rate ratios (Fig. 7A). At the outset, the flow rate ratio between disperse and continuous phases was varied. Increasing the flow rate ratio to or above 1 : 5 (alginate : sunflower oil) produced visibly discrete spherical beads (Fig. 7B). The hydrogel beads formed at lower ratios of 1 : 3 and 1 : 4 were interconnected, whereas ratios of 1 : 5 and 1 : 10 formed consistently distinct alginate beads throughout the process. By testing four conditions with varying flow rates of both the continuous and disperse phases, the flow rate ratio of 1 : 10 was selected for further optimisation of bead size and homogeneity (Fig. 7C). The hydrogel beads formed at each flow rate were measured by laser diffraction, and the D10, D50 and D90 percentiles by volume were calculated (Fig. 7D and E). Increasing flow rate proportionally increased the D50 value of the resulting alginate beads, with those formed at a total rate of 110 µL min^{-1} averaging 55.70 ± 18.42 µm compared with those at 440 µL min^{-1} at 215.56 ± 0.52 µm. Further, while the low flow rate in Condition 1 produced a large distribution in particle diameter with three distinct size classes, the higher flow rate in Condition 4 generated beads with a narrow diameter distribution and a single distinct size class. Increasing the total flow rate considerably impacted alginate bead diameter, where the mean particle size as measured by microscopy ranged from 312.55 µm ± 122.56 (20 µL min^{-1} : 200 µL min^{-1}) to 134.20 µm ± 65.50 (30 µL min^{-1} : 300 µL min^{-1}) (Fig. 7F). Notably, the lower flow rates in conditions 1 and 2 generated alginate beads with a cone-like morphology, whereas beads produced at higher flow rates were spherical.

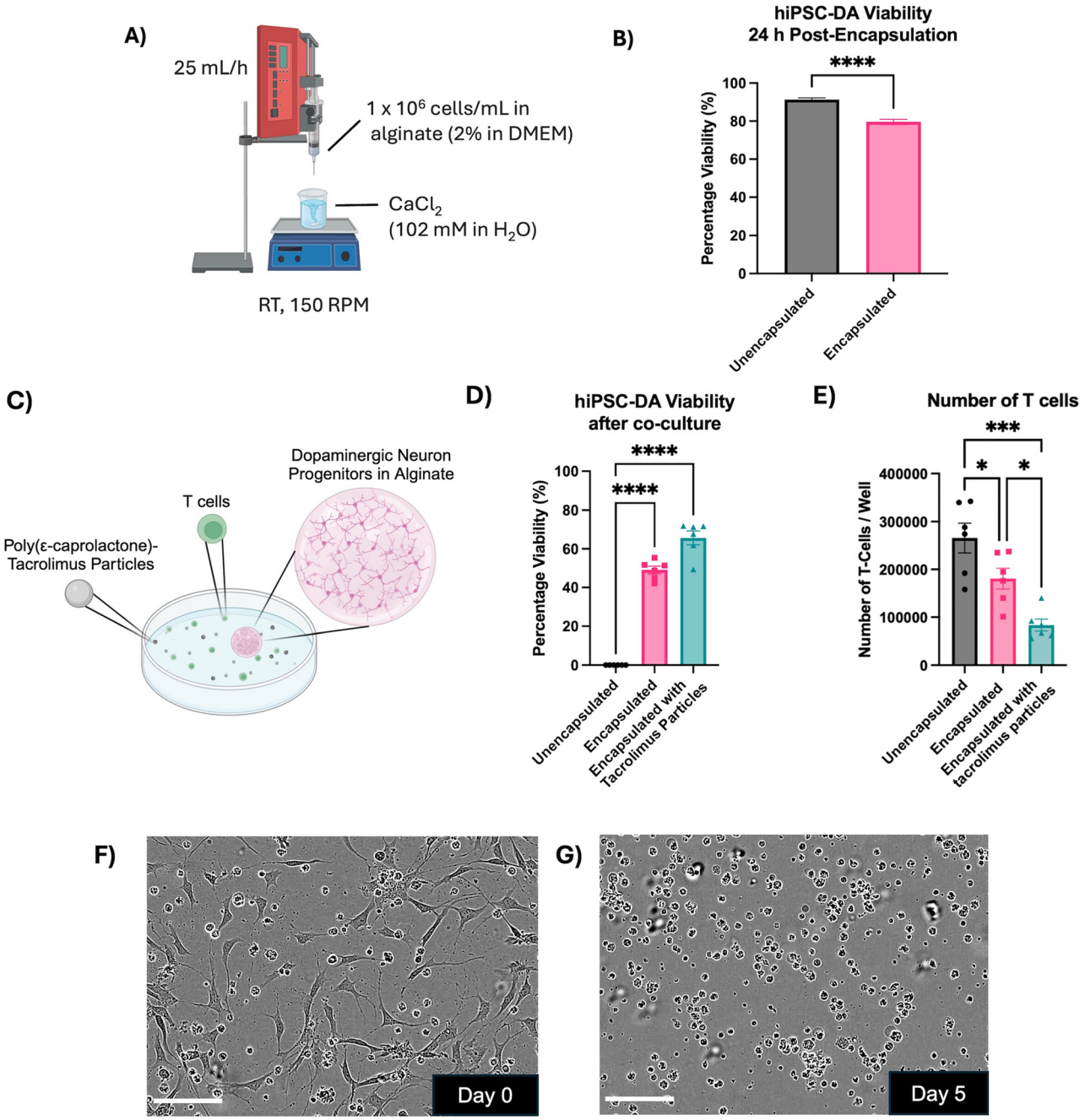

Fig. 5 Immunomodulatory encapsulation system protects dopaminergic progenitors and reduces T cell activation in an *in vitro* model of immune response. (A) Schematic of the method for encapsulation of day 16 dopaminergic progenitors in alginate beads. (B) Viability of day 16 hiPSC-derived dopaminergic progenitors 24 h after encapsulation in alginate beads (two-tailed *T* test, n = 15 alginate beads or n = 6 wells from three independent experiments, mean ± SEM, **** $p < 0.0001$). (C) Schematic of *in vitro* immune response assay where dopaminergic neuron progenitors were encapsulated in alginate and cultured with tacrolimus-loaded microparticles (25 μg mL^{-1}) and reactive T cells (40 000 per well) for five days. (D) Viability of dopaminergic progenitors after five-day exposure to reactive human T cells (one-way ANOVA with Dunnett's multiple comparisons test, n = 6 alginate beads from two independent experiments, mean ± SEM, **** $p < 0.0001$). (E) Number of T cells per well after five days in culture (one-way ANOVA with Tukey's *post-hoc* test, n = 6 wells per condition from two independent experiments, mean ± SEM, * $p < 0.05$ and *** $p < 0.001$). (F) and (G) Phase contrast micrographs of the unencapsulated dopaminergic neuron progenitor and T cell coculture under ×20 magnification on day 0 and day 5. Scale bar = 100 μm.

Discussion

Day 16 dopaminergic progenitors were used in this study since equivalent cells have been shown to improve outcomes following neural transplantation in rat models of Parkinson's disease,[26] and are currently being tested in clinical trials to treat Parkinson's disease patients.[27,28] An established protocol was adapted to differentiate hiPSCs into day 16 dopaminergic

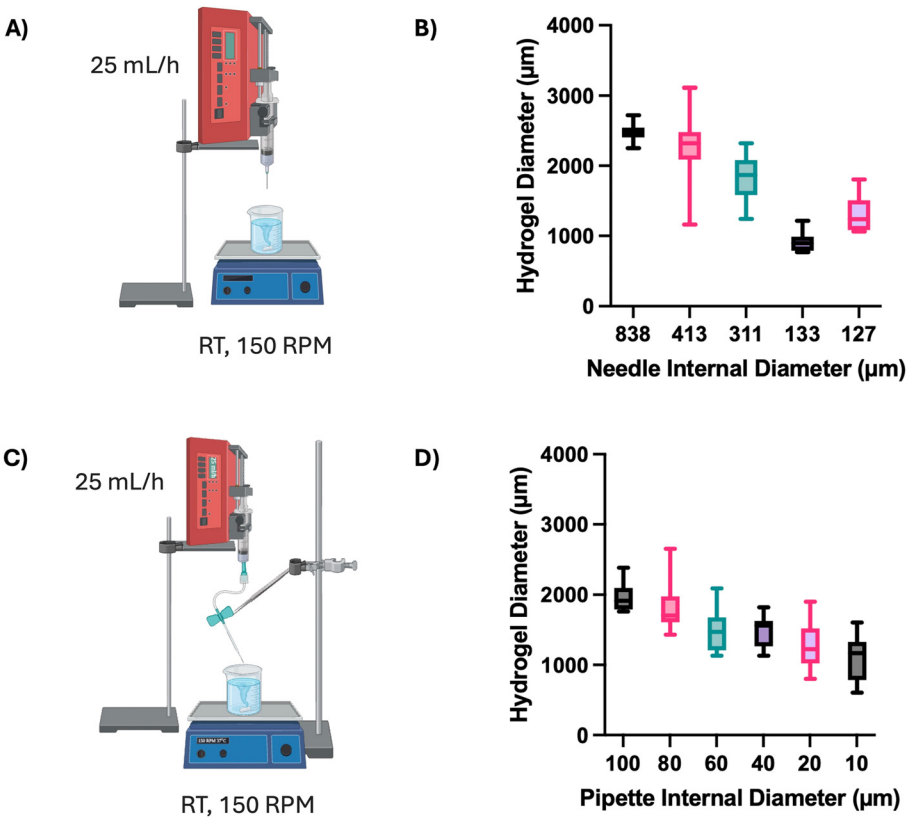

Fig. 6 Development of alginate bead encapsulation system. (A) Schematic of alginate bead production with dropwise release from a needle. (B) Effect of needle internal diameter on alginate bead size (n = 20 beads per condition, central line = median, box = upper and lower quartiles). (C) Schematic of alginate bead production with dropwise release from a pulled glass pipette. (D) Effect of pipette internal diameter on alginate bead size (n = 10 beads per condition).

progenitors and these were also further differentiated into dopaminergic neurons (day 35) for *in vitro* confirmation of functionality.[7,8] This method was based on passing the cells through the floor plate stage, critical in the embryonic development of midbrain dopaminergic neurons.[29–31] Immunocytochemical characterisation demonstrated that the hiPSCs expressed the transcription factor Oct4, which confirmed that the cells were pluripotent prior to differentiation.[32] The cells also expressed Nestin, a cytoplasmic intermediate filament protein involved in the stabilisation of cytoskeletal architecture. Nestin is predominantly expressed by neural progenitors in the human brain, although it has also been detected elsewhere in both the brain,[33] and other body tissues (reviewed in ref. 34). By day 16 the cells extended projections and were positive for βIII-tubulin,[35] indicating that these day 16 progenitors were of neuronal phenotype. Furthermore, the dopaminergic neuron progenitors also displayed expression of tyrosine hydroxylase, an enzyme critical for the synthesis of dopamine, and LMX1A, a marker commonly used to identify mesencephalic dopaminergic progenitors,[7] with nuclear localisation. At day 35, mature dopaminergic neurons were also positive for βIII-tubulin and LMX1A, and were confirmed to release dopamine *in vitro*. This is consistent with other reports demonstrating dopamine production in hiPSC-derived neurons at this timepoint.[36,37]

Cytokine and chemokine levels were compared across the three differentiation stages. Secretion of the pro-inflammatory cytokine CCL5 was greatest in hiPSCs compared with differentiated cells, in line with a previous study.[38] The homeostatic cytokine CXCL12 was elevated in the secretome of day 16 progenitors. This cytokine is expressed in the developing midbrain, the adult brain, and plays a role in the migration of A9 and A10 dopaminergic neurons.[39,40] Secretion of the pro-inflammatory cytokine IL-1β was detected from the hiPSCs, which is also reported elsewhere,[41] but was not detected in the differentiated cells. The CD40 ligand was elevated in the secretome of the hiPSCs and day 16 differentiated cells but not in the secretome of day 35 hiPSC-derived neurons. This was of particular note in this study as CD40 is involved in T cell regulation.[42] Future studies could explore how cytokines from transplanted progenitors influence the host immune response, informing immunosuppression requirements.

As an approach to provide local immunosuppression to improve transplanted cell survival, polymeric microparticles loaded with tacrolimus were generated. Tacrolimus is widely used for immunosuppression, where it suppresses the acti-

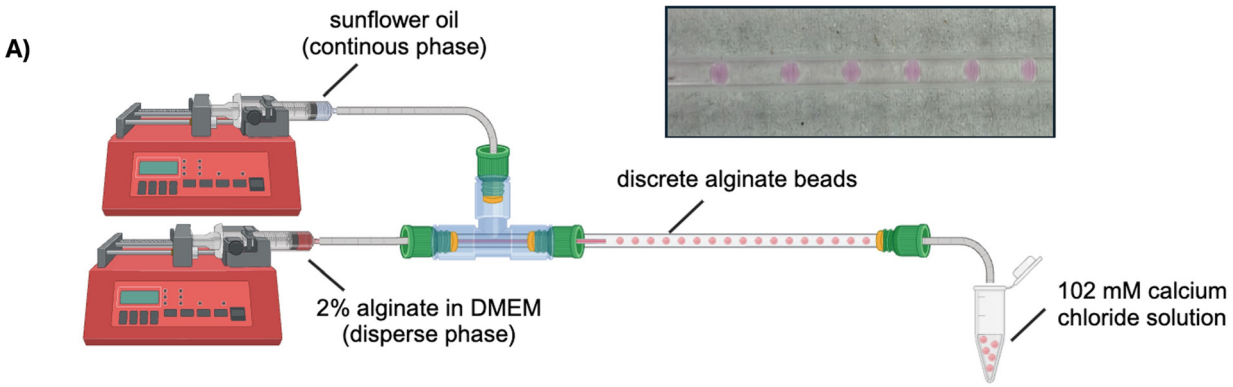

B)

Flow Rate (µL/min)		Flow Rate Ratio	Discrete Particles
Alginate (Disperse phase)	Sunflower Oil (Continuous phase)		
33	100	1:3	N
25	100	1:4	N
20	100	1:5	Y
10	100	1:10	Y

C)

Condition	Flow Rate (µL/min)		Flow Rate Ratio
	Alginate (Disperse phase)	Sunflower Oil (Continuous phase)	
1	10	100	1:10
2	20	200	1:10
3	30	300	1:10
4	40	400	1:10

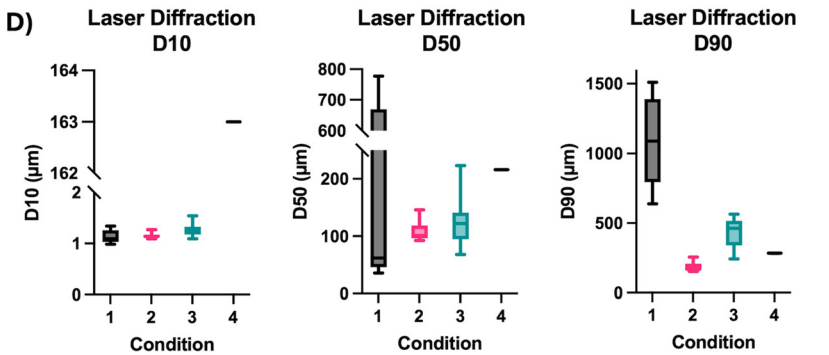

Condition	Laser Diffraction Hydrogel Diameter (µm)		
	D10	D50	D90
1	1.07 ± 0.07	55.70 ± 18.42	956.33 ± 274.52
2	1.15 ± 0.05	107.90 ± 17.36	184.00 ± 33.44
3	1.26 ± 0.13	124.74 ± 43.99	432.44 ± 106.48
4	163.00 ± 0.00	215.56 ± 0.52	283.11 ± 0.60

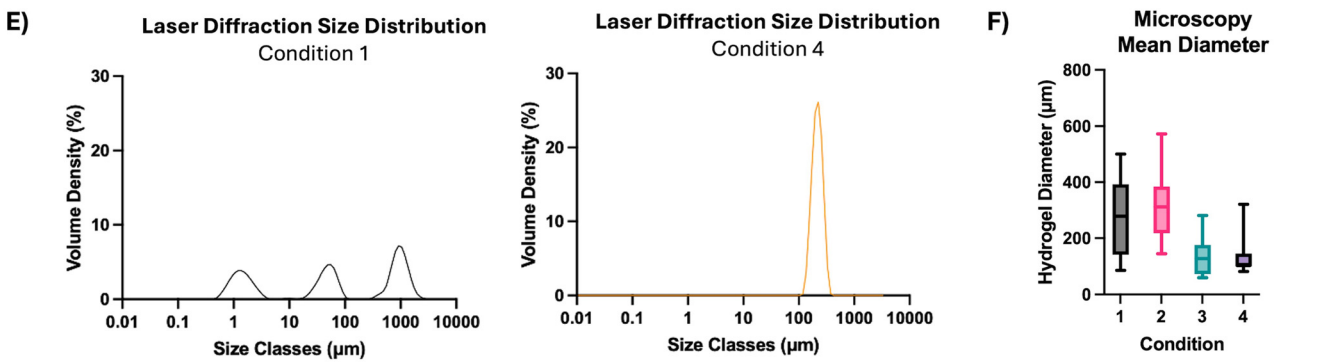

Fig. 7 Development of coaxial reactor conditions to yield monodisperse alginate beads. (A) Schematic of alginate bead production using a coaxial flow reactor developed in-house. Image of distinct alginate beads in glass capillary. (B) Table detailing the effect of flow rate ratio between disperse and continuous phases on formation of discrete beads. (C) Table detailing the flow rates used to optimise the diameter of the alginate beads. (D) D10, D50 and D90 measurements and (E) size distribution of alginate beads, as determined by laser diffraction (n = 9 measurements). (F) Effect of total flow rate on alginate bead size determined by microscopy (n = 10 beads per condition, central line = median, box = upper and lower quartiles and whiskers represent the minimum and maximum values).

vation and proliferation of T lymphocytes through calcineurin inhibition.[43] It may also offer other beneficial effects in the context of treating Parkinson's disease, having been linked with protection and improved survival of dopaminergic neurons.[44,45] The drug-loaded microparticles had an average diameter of 7 µm, which would allow them to readily pass

through the delivery needles with diameters around 1000 μm employed in recent clinical trials.[13,16,27] Steady release of tacrolimus was sustained from the microparticles for at least three weeks, which tends towards zero-order kinetics. This formulation has advantages over the use of tacrolimus-loaded nanoparticles that exhibited an initial burst release.[20] The optimal dose of tacrolimus required for local immunosuppression is yet to be determined. Most studies using systemic immunosuppression aim to maintain a plasma concentration of 5–15 ng mL^{-1} but do not report the concentration of tacrolimus at a tissue level.[46] Tacrolimus and other immunosuppressants are commonly delivered for 6–12 months post-transplantation in clinical studies, however, *in vitro* assessment of the immunogenicity of the cell therapy product used in the STEM-PD clinical trial has suggested that aggressive, long-term immunosuppression of this nature may not be required.[47]

As an approach to provide physical protection to improve cell transplantation, hiPSC-derived dopaminergic progenitors were encapsulated within alginate hydrogel beads, where they maintained high viability over 24 hours. Cell survival within the beads suggested that the encapsulation process was not overtly detrimental to viability and that the formed hydrogel structure permitted the exchange of oxygen and nutrients in culture. Crosslinked alginate has previously been shown to improve the viability of other injected cells when used as a carrier *versus* media alone.[48] This feature may be valuable for improving the outcomes of cell transplantation through physical protection during the procedure as well as immunoisolation of the graft.

To model key aspects of the host immune response to allogeneic grafts, the dopaminergic progenitors were exposed to cultures of human T cells. Encapsulation in alginate beads appeared to protect the progenitors from immune cell-mediated death and the addition of tacrolimus microparticles further bolstered their survival. This demonstrated that the beads effectively provided a barrier between encapsulated cells and the T cells, a major principle of immunoisolation by microencapsulation.[49] The increase in the number of T cells was considerably reduced in conditions with alginate-encapsulated progenitors. This finding is in line with previous work illustrating that alginate microencapsulation prevents the direct activation of cytotoxic $CD8^+$ T cells.[50] In our study this action was compounded in the presence of tacrolimus microparticles, an outcome in line with the expected pharmacological action of tacrolimus released from the polymer matrix. This confirmed that tacrolimus was released from the microparticles at a therapeutic concentration.

Having demonstrated the utility of encapsulating hiPSC-derived dopaminergic progenitors in alginate beads, the manufacturing process was optimised to improve the consistency and reduce the size of the hydrogel beads. Employing needles and pulled pipettes of decreasing diameter yielded a decrease in hydrogel bead diameter, down to a minimum size of ~800 μm. This restricted minimum diameter may be explained by Tate's law,[51] which implies a limit to droplet size based on the force balance between the droplet's gravity and the capillary force, and can be calculated using approximated values (eqn (S1)–(4) and Table S3†). Indeed, the predicted minimum hydrogel diameter under this law in this system is 775 μm, a bead size which may be too large for intracranial transplantation.

Using a coaxial flow reactor with sunflower oil as the continuous phase,[52] alginate bead size was substantially reduced and homogeneity improved, yielding beads with a clinically relevant diameter of ~100–200 μm. Other researchers have made similar-sized particles using alternative microfluidic devices and other reagents,[53,54] but the approach developed here uses milder reagents. The current method included a washing step that used hexane, but this could be avoided by substituting the sunflower oil with a biocompatible oil such as Fluo-Oil 7500. This oil is commonly used in microfluidic droplet formation and would not need to be washed away following particle production.[55] This would potentially streamline the manufacturing process of the particles. Although challenges may be faced when scaling up microfluidic particle production, the mass production of microscopic particles for biological delivery is feasible and has been reviewed in depth.[56]

Future work should explore the scale-up of the components within the immunomodulatory encapsulation system for clinical translation using Good Manufacturing Process (GMP) materials and processes. Moving forward, the biomaterial technology described here should be tested in an *in vivo* model to explore the effects on secreted factors, host immune response and transplanted cell survival. Though we developed this immunomodulatory encapsulation system with Parkinson's disease in mind, the technology has the potential to be adapted to other applications in regenerative medicine, for example, cell transplantation to treat Huntington's disease.[57,58] The technology can be applied by tailoring the stiffness of the hydrogel for the desired delivery location, selecting a clinically relevant cell type and optimising the tacrolimus-loaded particles for the desired release profile.

Conclusion

This study reported the further development and refinement of a cell encapsulation system based on alginate and immunosuppressant-loaded microparticles, for the delivery and protection of therapeutic cells in Parkinson's disease. The technology was designed to produce alginate hydrogel beads loaded with dopaminergic neuron progenitors and tacrolimus-loaded microparticles. The aim was to simultaneously shield donor cells from the host immune system and potentially circumvent the current requirement for systemic immunosuppression in patients receiving therapeutic cell transplants. The efficacy of the immunomodulatory system was assessed *in vitro* through exposure to T cells, where significantly greater survival of dopaminergic progenitors was observed with alginate encapsulation and the presence of tacrolimus microparticles. The T cell response was 3-fold lower with the inclusion of the encapsulation system. In addition, a coaxial flow reactor was used to

manufacture highly consistent alginate hydrogel beads with a median diameter of 215.6 ± 0.5 μm, potentially suitable for the delivery of therapeutic cells with local immunosuppression in humans.

Author contributions

EAA: conceptualisation, methodology, formal analysis, investigation, writing – original draft, writing – review and editing, vsualization. HG: methodology, formal analysis, investigation, writing – original draft. REE: conceptualisation, methodology, investigation. LNC: investigation, methodology. JBP: conceptualisation, supervision, writing – review and editing. RD: supervision, writing – review and editing, methodology. VHR: conceptualisation, supervision, writing – review and editing.

Data availability

The data supporting this article have been included as part of the ESI.† Any further data can be provided upon request.

Conflicts of interest

None of the authors have any conflict of interest to declare.

Acknowledgements

EA was supported by funding from EPSRC through the Centre for Doctoral Training in Transformative Pharmaceutical Technologies (EP/S023054/1) and REE was supported by funding from EPSRC through the Centre for Doctoral Training in Advanced Therapeutics & Nanomedicines (EP/L01646X/1). VR and HG were partly supported by funding from the 2018 UCL Rosetrees Stoneygate Prize and the Rosetrees Trust.

The authors are grateful to Shuting Li for her assistance in setting up the microfluidics system and John Frost, Senior Mechanical Workshop Technician, for providing some of the parts. Valuable advice about microparticle formulation was kindly provided by Dr I-Ning Lee and Dr Lisa White at the University of Nottingham.

References

1 B. R. Bloem, M. S. Okun and C. Klein, *Lancet*, 2021, **397**, 2284–2303.
2 K. R. Chaudhuri, D. G. Healy, A. H. Schapira and E. National Institute for Clinical, *Lancet Neurol.*, 2006, **5**, 235–245.
3 E. R. Dorsey and B. R. Bloem, *JAMA Neurol.*, 2018, **75**, 9–10.
4 T. B. Stoker, N. F. Blair and R. A. Barker, *Neural Regener. Res.*, 2017, **12**, 389–392.
5 R. A. Barker, A. Björklund and M. Parmar, *BioEssays*, 2024, 2400118, DOI: **10.1002/bies.202400118**.
6 M. Parmar, S. Grealish and C. Henchcliffe, *Nat. Rev. Neurosci.*, 2020, **21**, 103–115.
7 A. Kirkeby, S. Grealish, D. A. Wolf, J. Nelander, J. Wood, M. Lundblad, O. Lindvall and M. Parmar, *Cell Rep.*, 2012, **1**, 703–714.
8 S. Nolbrant, A. Heuer, M. Parmar and A. Kirkeby, *Nat. Protoc.*, 2017, **12**, 1962–1979.
9 Z. Alekseenko, J. M. Dias, A. F. Adler, M. Kozhevnikova, J. A. van Lunteren, S. Nolbrant, A. Jeggari, S. Vasylovska, T. Yoshitake, J. Kehr, M. Carlen, A. Alexeyenko, M. Parmar and J. Ericson, *Nat. Commun.*, 2022, **13**, 3046.
10 S. Grealish, E. Diguet, A. Kirkeby, B. Mattsson, A. Heuer, Y. Bramoulle, N. Van Camp, A. L. Perrier, P. Hantraye, A. Bjorklund and M. Parmar, *Cell Stem Cell*, 2014, **15**, 653–665.
11 T. Kikuchi, A. Morizane, D. Doi, H. Magotani, H. Onoe, T. Hayashi, H. Mizuma, S. Takara, R. Takahashi, H. Inoue, S. Morita, M. Yamamoto, K. Okita, M. Nakagawa, M. Parmar and J. Takahashi, *Nature*, 2017, **548**, 592–596.
12 D. Doi, H. Magotani, T. Kikuchi, M. Ikeda, S. Hiramatsu, K. Yoshida, N. Amano, M. Nomura, M. Umekage, A. Morizane and J. Takahashi, *Nat. Commun.*, 2020, **11**, 3369.
13 A. Kirkeby, J. Nelander, D. B. Hoban, N. Rogelius, H. Bjartmarz, R. Novo Nordisk Cell Therapy, P. Storm, A. Fiorenzano, A. F. Adler, S. Vale, J. Mudannayake, Y. Zhang, T. Cardoso, B. Mattsson, A. M. Landau, A. N. Glud, J. C. Sorensen, T. P. Lillethorup, M. Lowdell, C. Carvalho, O. Bain, T. van Vliet, O. Lindvall, A. Bjorklund, B. Harry, E. Cutting, H. Widner, G. Paul, R. A. Barker and M. Parmar, *Cell Stem Cell*, 2023, **30**, 1299–1314.
14 V. H. Roberton and J. B. Phillips, in *International Review of Neurobiology*, ed. E. L. Lane, C. J. G. Drew and M. J. Lelos, Academic Press, 2022, vol. 166, pp. 191–205.
15 S. Qarin, S. K. Howlett, J. L. Jones and R. A. Barker, *Neuronal Signaling*, 2021, **5**, NS20200083.
16 R. A. Barker and T. Consortium, *Nat. Med.*, 2019, **25**, 1045–1053.
17 C. E. Staatz and S. E. Tett, *Clin. Pharmacokinet.*, 2004, **43**, 623–653.
18 M. A. Bochenek, O. Veiseh, A. J. Vegas, J. J. McGarrigle, M. Qi, E. Marchese, M. Omami, J. C. Doloff, J. Mendoza-Elias, M. Nourmohammadzadeh, A. Khan, C. C. Yeh, Y. Xing, D. Isa, S. Ghani, J. Li, C. Landry, A. R. Bader, K. Olejnik, M. Chen, J. Hollister-Lock, Y. Wang, D. L. Greiner, G. C. Weir, B. L. Strand, A. M. A. Rokstad, I. Lacik, R. Langer, D. G. Anderson and J. Oberholzer, *Nat. Biomed. Eng.*, 2018, **2**, 810–821.
19 G. Basta, P. Montanucci, G. Luca, C. Boselli, G. Noya, B. Barbaro, M. Qi, K. P. Kinzer, J. Oberholzer and R. Calafiore, *Diabetes Care*, 2011, **34**, 2406–2409.
20 D. Eleftheriadou, R. E. Evans, E. Atkinson, A. Abdalla, F. K. H. Gavins, A. S. Boyd, G. R. Williams, J. C. Knowles, V. H. Roberton and J. B. Phillips, *RSC Adv.*, 2022, **12**, 4005–4015.

21 R. D. Bartlett, D. Eleftheriadou, R. Evans, D. Choi and J. B. Phillips, *Biomaterials*, 2020, **258**, 120303.
22 F. Brandl, F. Sommer and A. Goepferich, *Biomaterials*, 2007, **28**, 134–146.
23 M. C. Catoira, L. Fusaro, D. Di Francesco, M. Ramella and F. Boccafoschi, *J. Mater. Sci.: Mater. Med.*, 2019, **30**, 115.
24 B. Snow, E. Mulroy, A. Bok, M. Simpson, A. Smith, K. Taylor, M. Lockhart, B. J. Lam, C. Frampton, P. Schweder, B. Chen, G. Finucane, A. McMahon and L. Macdonald, *Parkinsonism Relat. Disord.*, 2019, **61**, 88–93.
25 C. A. Schneider, W. S. Rasband and K. W. Eliceiri, *Nat. Methods*, 2012, **9**, 671–675.
26 B. M. Hiller, D. J. Marmion, C. A. Thompson, N. A. Elliott, H. Federoff, P. Brundin, V. B. Mattis, C. W. McMahon and J. H. Kordower, *npj Regener. Med.*, 2022, **7**, 24.
27 J. Takahashi, *Regener. Ther.*, 2020, **13**, 18–22.
28 *Nat. Biotechnol.*, 2023, **41**, 1183.
29 S. Mesman and M. P. Smidt, *Int. J. Mol. Sci.*, 2020, **21**, 4638.
30 Y. Ono, T. Nakatani, Y. Sakamoto, E. Mizuhara, Y. Minaki, M. Kumai, A. Hamaguchi, M. Nishimura, Y. Inoue, H. Hayashi, J. Takahashi and T. Imai, *Development*, 2007, **134**, 3213–3225.
31 A. Kirkeby, J. Nelander and M. Parmar, *Front. Cell. Neurosci.*, 2012, **6**, 64.
32 Z. Simandi, A. Horvath, L. C. Wright, I. Cuaranta-Monroy, I. De Luca, K. Karolyi, S. Sauer, J. F. Deleuze, L. J. Gudas, S. M. Cowley and L. Nagy, *Mol. Cell*, 2016, **63**, 647–661.
33 M. L. Hendrickson, A. J. Rao, O. N. Demerdash and R. E. Kalil, *PLoS One*, 2011, **6**, e18535.
34 A. Bernal and L. Arranz, *Cell. Mol. Life Sci.*, 2018, **75**, 2177–2195.
35 A. J. I. Roskams, X. Cai and G. V. Ronnett, *Neuroscience*, 1998, **83**, 191–200.
36 S. Mahajani, A. Raina, C. Fokken, S. Kugler and M. Bahr, *Cell Death Dis.*, 2019, **10**, 898.
37 E. M. Hartfield, M. Yamasaki-Mann, H. J. Ribeiro Fernandes, J. Vowles, W. S. James, S. A. Cowley and R. Wade-Martins, *PLoS One*, 2014, **9**, e87388.
38 M. Gao, H. Yao, Q. Dong, H. Zhang, Z. Yang, Y. Yang, J. Zhu, M. Xu and R. Xu, *Sci. Rep.*, 2016, **6**, 29955.
39 S. Yang, L. C. Edman, J. A. Sánchez-Alcañiz, N. Fritz, S. Bonilla, J. Hecht, P. Uhlén, S. J. Pleasure, J. C. Villaescusa, O. Marín and E. Arenas, *Development*, 2013, **140**, 4554–4564.
40 G. O. Bodea, J.-H. Spille, P. Abe, A. S. Andersson, A. Acker-Palmer, R. Stumm, U. Kubitscheck and S. Blaess, *Development*, 2014, **141**, 661–673.
41 L. Tamò, K. Fytianos, F. Caldana, C. Simillion, A. Feki, I. Nita, M. Heller, T. Geiser and A. Gazdhar, *Int. J. Mol. Sci.*, 2021, **22**, 958.
42 H. Choi, H.-J. Lee, H.-J. Sohn and T.-G. Kim, *BMC Immunol.*, 2023, **24**, 15.
43 O. M. Noceti, J. B. Woillard, A. Boumediene, P. Esperon, J. L. Taupin, S. Gerona, M. Valverde, C. Tourino and P. Marquet, *Clin. Chem.*, 2014, **60**, 1336–1345.
44 A. K. Wright, C. Miller, M. Williams and G. Arbuthnott, *Brain Res.*, 2008, **1216**, 78–86.
45 R. F. Castilho, O. Hansson and P. Brundin, *Exp. Neurol.*, 2000, **164**, 94–101.
46 E. C. Toll, A. M. Seifalian and M. A. Birchall, *Regener. Med.*, 2011, **6**, 635–652.
47 A. J. Curle, S. V. Fazal, S. Qarin, S. K. Howlett, X. He, R. A. Barker and J. L. Jones, *bioRxiv*, 2024, 2024.2001.2023.576826,DOI: **10.1101/2024.01.23.576826**.
48 B. A. Aguado, W. Mulyasasmita, J. Su, K. J. Lampe and S. C. Heilshorn, *Tissue Eng., Part A*, 2012, **18**, 806–815.
49 G. A. Paredes Juarez, M. Spasojevic, M. M. Faas and P. de Vos, *Front. Bioeng. Biotechnol.*, 2014, **2**, 26.
50 Y. Li, A. W. Frei, E. Y. Yang, I. Labrada-Miravet, C. Sun, Y. Rong, M. M. Samojlik, A. L. Bayer and C. L. Stabler, *Biomaterials*, 2020, **256**, 120182.
51 T. Tate, *London, Edinburgh Dublin Philos. Mag. J. Sci.*, 1864, **27**, 176–180.
52 A. A. Dias Meirelles, A. L. Rodrigues Costa, M. Michelon, J. Viganó, M. S. Carvalho and R. L. Cunha, *J. Food Eng.*, 2022, **315**, 3385.
53 S. Utech, R. Prodanovic, A. S. Mao, R. Ostafe, D. J. Mooney and D. A. Weitz, *Adv. Healthcare Mater.*, 2015, **4**, 1628–1633.
54 V. L. Workman, S. B. Dunnett, P. Kille and D. D. Palmer, *Biomicrofluidics*, 2007, **1**, 14105.
55 T. Tang, H. Zhao, S. Shen, L. Yang and C. T. Lim, *Microsyst. Nanoeng.*, 2024, **10**, 3.
56 H. Lin, J. Leng, P. Fan, Z. Xu and G. Ruan, *Mater. Adv.*, 2023, **4**, 2885–2908.
57 A. E. Rosser, C. M. Kelly and S. B. Dunnett, *Future Neurol.*, 2010, **6**, 45–62.
58 M. Csobonyeiova, S. Polak and L. Danisovic, *Int. J. Mol. Sci.*, 2020, **21**, 2239.